JACS
JOURNAL OF THE AMERICAN CHEMICAL SOCIETY

ARTICLE

pubs.acs.org/JACS

Fluoride-Rich, Hydrofluorothermal Routes to Functional Transition Metal (Mn, Fe, Co, Cu) Fluorophosphates

Jennifer A. Armstrong, Edward R. Williams, and Mark T. Weller*

School of Chemistry, University of Southampton, Southampton. SO17 1BJ. U.K.

Supporting Information

ABSTRACT: Hydrofluorothermal methods are shown to offer a facile route to a very large family of mid-late first row, transition metal fluorophosphates with 50 new compounds identified to date for manganese(III), iron(III), cobalt(II), and copper(II). Reactions of a transition metal fluoride with a phosphate source in a very low-water, high-fluoride content system and in the presence of framework charge balancing metal cations or template molecular cations, lead to materials with structures formed from linked $M(O,F)_n$ and $P(O,F)_n$ polyhedra. The structures of these materials, which contain a variety of 1, 2, and 3-dimensional motifs with a level of framework termination dependent upon their fluoride content, show numerous useful characteristics for functionality and applications. The new and unusual features of these fluorophosphate materials include interlayer spaces or channels lined with fluoride ions, metal polyhedra, $M(O,F)_n$, linked through vertex, edge, or face-sharing, and μ^2, μ^3, and μ^4 bridging fluoride ions. Preliminary characterization of the properties of some of these metal fluorophosphates is reported, including reductive lithium ion insertion, of interest for Li-ion battery positive electrodes, ion exchange reactions, the formation of nanoporous material derivatives through template destruction, and magnetic susceptibility behaviors.

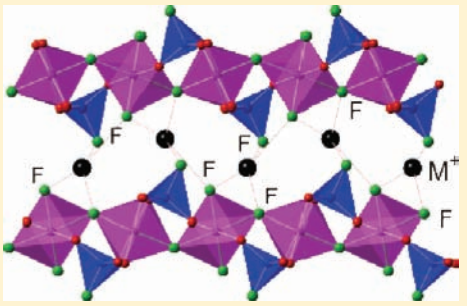

1. INTRODUCTION

Inorganic framework materials formed from linked polyhedral units are of great importance owing to their widespread applications as, for example, ion exchangers, battery materials, catalysts, nonlinear optics, and gas storage/adsorption materials.[1] Porous framework structures based on linked oxotetrahedral units constitute an important subclass in the field of materials chemistry as exemplified by aluminosilicate zeolites[2] and aluminophosphates.[3] Further structural diversity and enhanced functionality derives from the use of metals as MO_n units with additional structural motifs beyond tetrahedral co-ordination, and linking of these various polyhedral building blocks leads to zero dimensional clusters, one-dimensional (1D) chains, two-dimensional (2D) clay-like layer structures,[4] and semicondensed and open three-dimensional (3D) frameworks.[5] In the latter class of 3D framework, materials with small channels, such as $LiFePO_4$[6] and $A_xM_2(XO_4)_3$ (NASCION type materials),[7] are of importance as Li-ion battery materials and cationic conductors, respectively, while more open structure materials, such as the titanosilicates[8] and zirconium phosphates,[4,9] are used in ion exchange and catalysis applications.

Incorporation of fluoride into the metal phosphate framework structures, effectively replacing oxide by fluoride on a metal or phosphorus site, changes both the structural and compositional aspects of the chemistry. Factors here include the propensity of F^- compared with O^{2-} in bridging different transition metal centers and the formation of terminal fluoride sites on $[MO_nF_{6-n}]^{m-}$ and $[PO_{4-p}F_p]^{q-}$ polyhedra; variation in composition therefore allows the control of structural dimensionality and how the polyhedra are linked, that is through vertex, edge, or face sharing, or terminated. In addition the electron-withdrawing/sigma donor character of the F^- ion means that reactions in fluoride rich media have the ability to stabilize higher oxidations states on a transition metal.

Many materials containing mid- to late-first row transitional metals have applications that would benefit from a greater ability to control structure, oxidation state, and composition through, for example, incorporation of fluoride. One example is in the development of Li-ion battery materials where mixed anion systems offer an extensive chemistry in the search for new cathode materials particularly as fluorophosphates exhibit high cell potentials as a result of both the inductive effect of PO_4^{3-} group and the electron-withdrawing character of the F^- ion.[10] A few fluorophosphate materials have recently been investigated for this application, including $LiVPO_4F$,[11] M_2FePO_4F, M = Na, Li, produced using high temperature conditions,[12] and a sodium vanadium fluorophosphate, $Na_3V_2(PO_4)_2F_3$.[13] Further interest in metal fluoro-compounds includes the condensed framework structures constructed of linked $[MO_xF_{6-x}]^{n-}$ ($x = 1$, $M = V^{5+}$, Nb^{5+}, Ta^{5+}, and $x = 2$, $M = Mo^{6+}$, W^{6+}) polyhedra which have been extensively studied with respect to their nonlinear optical properties,[13] magnetic materials (where exchange interactions through fluoride ion bridges between transition metal centers are modified with respect to those through oxide[14]), and in catalysis where changing fluoride to oxide can be used to control Lewis site acidity.[15] However, there has been very little work on

Received: February 4, 2011
Published: May 09, 2011

dx.doi.org/10.1021/ja201096b | J. Am. Chem. Soc. 2011, 133, 8252–8263

producing open and semicondensed framework materials where oxofluorotetrahedral units $T(O,F)_4^{n-}$ (T = P, Si, As, Ga, etc.) are combined with fluoride ions to link the important mid- to late-transition metal centers (Mn−Cu). Most of the reported work[16,17] has concentrated on aluminum, gallium, and fully oxidized group IV and V fluorophosphates where the important redox properties and cooperative magnetic behaviors are absent.

Until now the majority of transition metal oxide−fluoride framework compounds containing fluoride, such as those investigated for positive electrode materials and nonlinear optics, have been obtained through high temperature reaction chemistry. A much more versatile route to fluoride containing framework materials is a hydrofluorothermal method, where materials containing a transition metal, coordinated to fluoride and oxide, and more rarely, in combination with oxotetrahedral species such as PO_4 and PO_3F, can be obtained;[16] further structural and compositional flexibility with tetrahedral units is derived from the possible partial condensation and the formation of species such as the (fluoro-)pyrophosphates, $P_2(O,F)_7^{n-}$. Hydrothermal methods of incorporating low levels of fluoride into framework materials has been accomplished by several groups including the work of Férey and co-workers who by using HF as a mineralizer in hydrothermal reaction chemistry synthesized, perhaps serendipitously, a number of gallium fluorophosphate and iron fluorophosphate materials.[17,18] Synthesis in HF media, but without oxotetrahedra-forming units, leads to numerous templated structures with metal fluoro- or metal oxofluoro- frameworks, as recently reviewed by Lightfoot.[19] Early transition metal oxide fluorides, including some proposed for use as battery cathodes, can also be synthesized hydrothermally in the presence of HF, for example, $Ag_4V_2O_6F_2$.[20] To incorporate moderate to high levels of fluoride into a framework material together with an oxotetrahedral unit, such as PO_4^{3-} or PO_3F^{2-}, new synthesis strategies need to be adopted that maintain the high values of the fluoride/oxide molar ratio required to drive the formation of metal fluorophosphate compounds. We have previously reported that employing a metal fluoride as a starting material is an effective route for early transition metal fluorophosphate-frameworks,[16] including the use of structure directing species for producing nanoporous structures. Low temperature (<250 °C) reaction conditions also provide a route to compositional and structural features not readily available via high temperature methods including layer and channel structures; further advantages of hydro-(fluoro)thermal methods in producing functional materials, such as $LiFePO_4$, is that conditions can be tuned to generate small uniform particle sizes[21] and can be carried out as a continuous process.

Here we report the synthesis and structural characterization of approximately 50 mid- to late-first row transition metals (Mn to Cu) framework fluorophosphates produced in fluoride-rich hydrothermal media derived from the use of a metal fluoride as a reactant. As interest in the applications of these materials is likely to lie in the areas of improved positive-electrode materials, in their magnetic properties, and as nanoporous systems, preliminary investigations of some of the *chemie douce*, ion exchange, pyrolytic template destruction and Li-ion insertion chemistry, of the new metal fluorophosphates is also reported together with initial magnetic susceptibility measurements.

2. EXPERIMENTAL METHOD

A survey of fluoride-rich hydrofluorothermal chemistry using first row transition metal fluorides in combination with phosphoric and fluorophosphoric acids (H_3PO_4, 85 wt % in H_2O and HPF_6, 65 wt % in H_2O) was undertaken, Table 1. We report results for the starting materials MnF_3, FeF_3, CoF_3, and CuF_2; these metals are of importance for Li-ion battery material applications (particularly Co and, to a lesser extent, Fe and Mn), frequently demonstrate unusual magnetic properties (the Jahn−Teller d^4 (Mn(III)) and d^9 (Cu(II)) systems and Heisenberg 1-D systems (Cu(II))), and are of potential use in redox catalysis. Synthesis details, example reaction conditions and experimental methods are provided in Table 1 and as Supporting Information (S1). The surveyed range of reaction conditions, Table 1, included varying the metal fluoride/phosphate ratio and the use of a range of counter cations M^{n+} (added as MF_n or MOH; as a 50 wt % solution in H_2O (Rb,Cs), 45 wt % solution KOH, or 35% solution NH_3) or structure directing agents such as alkylammonium cations (added as pure amine to the reaction mixture). Product compositions were determined from the single crystal X-ray structure determinations and confirmed from SEM/EDAX analysis (see Supporting Information S2).

3. RESULTS

Table 1 summarizes the new transition metal fluorophosphates identified in this work, together with brief descriptions of their structures organized with respect to the dimensionality of the framework for each metal. In this article further details of eight of these structures are provided; these have been selected to illustrate the range, in terms of compositional and structural features, of transition metal fluorophosphates that can be obtained by this synthetic method. This is followed by a discussion of the general type of material produced in respect of their overall compositional and structural characteristics.

Metal Fluorophosphate 1; $(NH_4)_3Fe(III)_4F_9(PO_4)_2$. (Table 1, compound JFE32). The structure of $[(NH_4)_3]^{3+}[Fe(III)_4F_9(PO_4)_2]^{3-}$, Figure 1a, can be envisaged as being constructed from four FeO_2F_4 octahedra linked into tetrahedral units which then link further to form infinite chains along the crystallographic *a*-lattice direction; these chains are cross-linked through PO_4 units into a three-dimensional network defining channels containing the ammonium cations.

Metal Fluorophosphate 2; $(CH_3NH_3)FeFPO_4$. (Table 1, compound JFE123). The structure of $(CH_3NH_3)^+$ $[Fe(III)FPO_4]^-$, Figure 1b, consists of slightly corrugated infinite chains of *cis* and *trans* F-bridged FeO_4F_2 octahedra along *b*-lattice direction that are cross-linked by PO_4 tetrahedra to form a three-dimensional channel system containing methylammonium cations.

Metal Fluorophosphate 3; $(NH_4)(Co(II)_3F_2(P_2O_6F)_2)$. (Table 1, compound JCO152). The structure of $[NH_4]^+[Co(II)_3F_2(P_2O_6F)_2]^-$, Figure 2a, consists of CoO_6 octahedra sharing trans edges with two CoO_5F octahedra which then link into corrugated chains through skewed trans edge-sharing. These chains are then further linked into thick (9 Å) layers by ditetrahedral P_2O_6F fluoropyrophosphate anions, with the P−F bond directed into the interlayer region, separated by ammonium cations.

Metal Fluorophosphate 4; $[H_2$−*N*-(2-Aminoethyl)-1,3-propane-diamine$]_2$ $\{[Co(II)(PO_3F)]_4F[PO_2F_2]_2.(H_2O,F)\}$. (Table 1, JCO140). The structure of $[H_2$−*N*-(2-aminoethyl)-1,3-propanediamine$]_2[Co(II)(PO_3F)]_4F[PO_2F_2]_2.(H_2O,F)$, Figure 2b, consist of tetrahedral clusters centered on μ^4-fluoride and formed from four CoO_4F trigonal pyramids and bridged through the oxygen atoms of four PO_3F tetrahedra to form a distorted cubic unit of stoichiometry $[Co(II)(PO_3F)]_4F$. These clusters are linked through PO_2F_2 groups using the apical oxygen on the CoO_4F trigonal

dx.doi.org/10.1021/ja201096b |*J. Am. Chem. Soc.* 2011, 133, 8252–8263

Table 1. Summary of Transition Metal Fluorophosphates Identified in This Study with Compositions, Synthesis Conditions, Crystallographic Parameters, and Key Structural Features

product, (code)	synthesis conditions and product yield/purity	crystallographic structure: lattice type, space group, lattice parameters (Å) and (deg) and cell volume (Å^3)	key structure features[a]
$NH_4Co(II)_3F_2(P_2O_6F)_2$ (JCO152)	CoF_3 (0.0667 g) + H_3PO_4 (0.10 mL) + 2-(aminomethyl) pyridine (FW 108.14, d = 1.04; 0.12 mL) → 175 °C, 96 h. Major phase product ~60%. Yield = 0.0841 g.	monoclinic $P2_1/c$; a = 9.3460 b = 8.0993 c = 9.3100 β = 99.565; V = 696.93(6)	chains of edge sharing CoO_6 and CoO_5F octahedra linked by P_2O_6F pyrofluorophosphate groups into **2D** layers separated by NH_4^+ ions
$[H\text{-}DET]_2Co_3(PO_3(OH,F))_2O_2F_2$ (JCO209)	CoF_3 (0.0667 g) + HPF_6 (0.16 mL) + Diethylenetriamine (0.12 mL) → 175 °C, 96 h. Minor phase ~30%. Yield = 0.0196 g.	monoclinic $P21/c$; a = 10.3271 b = 10.7820 c = 7.3524 β = 100.252; V = 805.6	**2D** layers of $Co(O,F)_6$ edge and corner linked to form hexagonal rings and terminated by $(PO_3(OH,F))$ units directed into interlayer region. Protonated template molecules in hexagonal rings and between layers.
$(NH_4)Co(II)OPO_4$ (JCO119)	CoF_3 (0.0667 g) + H_3PO_4 (0.10 mL) + N-(3-aminopropyl)-1,3-propane diamine (0.16 mL) → 175 °C, 48 h. Single phase. Yield = 0.0820 g. Amine decomposes	orthorhombic $Pmn2_1$; a = 5.6061 b = 8.7770 c = 4.7753; V = 234.97	**2D** layers of CoO_6 octahedra with bidentate PO_4 units separated by ammonium ions.
$LiCo_2[P_2(O_{5.5}(OH,F)_{1.5})]_2$ (JCOJ010)	CoF_3 (0.0667 g) + H_3PO_4 (0.10 ml) + LiF (0.0298 g) → 225 °C, 48 h. Major phase product ~80%. Yield 0.1280 g.	Monoclinic $C2/c$; a = 10.9823 b = 12.7987, c = 8.9323 β = 123.059; V = 1052.26	Zig-zag chains of edge-sharing CoO_6 octahedra bridged and cross-linked by fluoro-pyrophosphate groups forming a **3D** framework with channels along the (101) direction containing Li^+ and empty channels along c.
$MCo(II)_3[PO_3(OH,F)]_2$-$[PO_2(OH,F)_2]F_2$; M = Rb (JCO3), K (JCO56), NH_4 (JCO110)	JCO3: CoF_3 (0.0667 g) + H_3PO_4 (0.10 mL) + RbOH (0.14 mL) → 175 °C, 48 h. Single phase. Yield = 0.0345 g. JCO56: CoF_3 (0.0667 g) + H_3PO_4 (0.10 mL) + KOH (0.10 mL) → 175 °C, 72 h. Major phase ≈ 70%. JCO110: CoF_3 (0.1334 g) + H_3PO_4 (0.10 mL) + NH_3 solution (0.03 mL) → 175 °C, 48 h. Single phase. Yield = 0.0461 g.	monoclinic $C2/c$; M = Rb a = 20.1634, b = 7.4574, c = 7.5081, β = 102.759; V = 1101.1; M = K a = 19.9875, b = 7.4105, c = 7.4952, β = 102.129; M = NH_4^+ a = 19.9583 b = 7.4583 c = 7.5395 β = 102.557.	face and edged sharing CoO_4F_2 octahedra linked by PO_3F units into 2D layers further cross-linked by PX_4 into **3D** structure with two orthogonal channels containing Rb^+, K^+ or NH_4^+ cations.
$BaCo(II)PO_4F$ (JCO57)	CoF_3 (0.0667 g) + H_3PO_4 (0.20 mL) + $Ba(OH)_2 \cdot 8H_2O$ (0.3628 g) → 175 °C, 72 h. Minor phase ~20%. Yield = 0.1925 g.	orthorhombic, $P2_12_12_1$; a = 4.7869 b = 9.0674 c = 9,.6550; V = 419.07	CoO_4F square-pyramids linked by PO_4 tetrahedra into a **3D** connected framework forming channels in two orthogonal directions containing Ba^{2+} ions. Long Co−O interactions at 2.72 Å
$[C_2N_2H_{9.5}]_2Co(II)_4F(PO_4)_2$-$(PO_3F)_2.H_2O$ (JCO59)	CoF_3 (0.0667 g) + H_3PO_4 (0.10 mL) + ethylenediamine (0.08 mL) → 175 °C, 72 h. Major phase ≈ 95%. 0.0520 g.	orthorhombic $Cmcm$ a = 14.8737 b = 9.6815 c = 13.6354; V = 1963.5	μ^4 bridged F- at the center of 2 x CoO_5F octahedra and 2x CoO_4F trigonal bipyramids, cross-linked by PO_4 and PO_3F tetrahedra into cubic units; these link to form a **3D** framework delineating as 2D orthogonal channel system containing protonated ethylenediamine ($C_2N_2H_n$) template molecules.

Table 1. Continued

product, (code)	synthesis conditions and product yield/purity	crystallographic structure: lattice type, space group, lattice parameters (Å) and (deg) and cell volume (Å^3)	key structure features[a]
$[H_{1.5}$ N-(2-aminoethyl)-1,3-propane-diamine$]_2^{3+}[Co(II)(PO_3F)]_4F[PO_2F_2]_2.H_2O$ (JCO140)	CoF_3 (0.0667 g) + H_3PO_4 (0.10 mL) + N-(2-aminoethyl)-1,3-propanediamine →175 °C, 48 h. 50% phase pure. Yield = 0.0852 g.	tetragonal $P4\bar{n}2$; a = 12.9197 c = 9.8491 V = 1644.0	tetrahedral/cubic clusters centered on μ^4 fluoride and formed from 4 × CoO_4F trigonal pyramids and 4 × PO_3F. Clusters linked through PO_2F_2 groups and apical oxygen on CoO_4F to form a **3D** framework with fully connected 3D channel system. Cavities contain protonated template and H_2O.
$[Amine]_x$. $Co(PO_4)$ (JCO183)	CoF_3 (0.0667 g) + H_3PO_4 (0.10 mL) + *N*-(3-Aminopropyl)-1,3-propanediamine (d = 0.938; 0.16 mL) → 175 °C, 96 h. 50% phase pure. Yield = 0.0819 g. Amine partially decomposes.	hexagonal $P6_3$; a = 10.7241 c = 8.7005; V = 866.56	**3D** framework isostructural with NH_4CoPO_4—HEX.[25]
$Co(II)_2PO_4F$ (JCO2)	CoF_3 (0.0667 g) + H_3PO_4 (0.10 mL) + CsOH (0.20 mL) → 175 °C, 48 h. Single phase. Yield = 0.0275 g.	monoclinic $C2/c$; a = 12.8559, b = 6.3968, c = 9.7035, β = 117.560; V = 707.43	Compact **3D** structure with corner and edge sharing CoO_4F_2 octahedra linked through PO_4 tetrahedra; fluoride ions disordered in chains along c.
$Co_5F_6(PO_3F)_4$ (JCO211)	CoF_3 (0.0667 g) + HPF_6 (0.16 mL) + cyclohexylamine (0.13 mL) → 175 °C, 96 h. 80% phase pure. Yield = 0.0473 g. Amine decomposes	orthorhombic $Cmca$; a = 8.5113 b = 18.6365 c = 9.9502; V = 1578.3	CoO_4F_2 octahedra sharing edges and vertices with a μ^3-F and further linked by disordered PO_3F tetrahedra into a **3D** framework with small 1D channel system (vacant).
$Co(II)_{3+x}(F,O)_2(PO_3F)_2$ (JCO130)	CoF_3 (0.0667 g) + H_3PO_4 (0.10 mL) + triethylamine (0.16 mL) → 175 °C, 48 h. Amine decomposes.	monoclinic $P2_1/c$,; a = 7.5369, b = 7.3936 c = 7.3923 β = 119.01; V = 360.27	triplets of face sharing CoO_4F_2 and CoO_2F_4 octahedra orthogonal chains linked by PO_3F in dense **3D** structure related to lipscombite[26] with almost fully ordered vacancies.
$Co(II)_{1.33}H_{1.33}PO_4F$ (JCO132 and JCO141)	JCO132: CoF_3 (0.0667 g) + H_3PO_4 (0.10 mL) + isobutylamine (0.12 mL) → 175 °C, 48 h JCO141: CoF_3 (0.0667 g) + H_3PO_4 (0.10 mL) + *N*-ethylmethylamine. Amines decompose.	tetragonal $I4_1/amd$; a = 5.2900 b = 12.9156; V = 361.43	**Dense 3D** Lipscombite structure type.[26] Face sharing CoO_4F_2 octahedra form orthogonal chains along a and b bridging fluoride and PO_4 groups. Cobalt sites $^2/_3$ occupied with OH groups around vacant sites.
$KMnF_2(PO_3(OH,F))_2$ (JMN50)	MnF_3 (0.0842 g) + H_3PO_4 (0.10 mL) + KOH (0.10 mL) → 175 °C, 72 h. Major crystalline phase ~70% remainder MnO_2 powder. Yield = 0.1335 g.	triclinic P-1;a = 4.8208 b = 8.2918 c = 10.7559 α = 89.620 β = 87.828 γ = 87.621; V = 429.26	MnF_2O_4 octahedra linked via $PO_3(OH,F)$ units into **1D** chains separated by K ions; Fe based and mixed metal systems, $K(Mn,Fe)F_2(PO_3(OH,F))_2$ also produced.
$Na_2MnF_3HPO_4$ (JMN9)	MnF_3 (0.0842 g) + H_3PO_4 (0.10 mL) + NaOH (0.06 mL) → 175 °C, 48 h. Minor crystalline phase ~25%, remainder MnO_2 powder Yield = 0.0532 g.	monoclinic $P2_1/m$; a = 5.6755 b = 7.7000 c = 6.8199 β = 109.734; V = 280.54	**2D** layers of MnO_2F_4 octahedra and $PO_3(OH)$ tetrahedra separated by Na^+ ions.
$Na_4Mn_2F_6(P_2O_7)$ (JMNJ15)	MnF_3 (0.0842 g) + H_3PO_4 (0.10 ml) + NaOH (0.06 mL) → 225 °C, 48 h. Major phase product ~70%, Yield 0.1080 g.	Monoclinic $P2/n$; a = 7.7805 b = 8.0834 c = 8.1265 β = 97.343	Chains formed of alternating MnO_4F_2 octahedra and doubly bridging pyrophosphate P_2O_7 cross-linked by MnF_4O_2 octahedra to form a 3**D** framework and 3**D** channel system containing Na^+.

Table 1. Continued

product, (code)	synthesis conditions and product yield/purity	crystallographic structure: lattice type, space group, lattice parameters (Å) and (deg) and cell volume (Å^3)	key structure features[a]
$Rb_2MnF_2(H_2PO_4)(HPO_4)$ (JMN11)	MnF_3 (0.0842 g) + H_3PO_4 (0.10 mL) + RbOH (0.14 mL) → 175 °C, 48 h. Single phase. Yield = 0.1470 g.	monoclinic $P2_1/c$; a = 7.3481 b = 7.8143 c = 8.5789 β = 114.36; V = 326.9	MnF_2O_4 octahedra linked via $PO_2(OH)_2$ units into **2D** sheets separated by Rb ions
$MMnF_2PO_3F$ ***M*** = **NH**$_4$ (JMN16), K (JMN102)	JMN16: MnF_3 (0.0842 g) + HPF_6 (0.16 mL) + NH_3 solution (0.03 mL) → 175 °C, 48 h. Single phase. Yield = 0.0484 g. JMN102: MnF_3 (0.1684 g) + H_3PO_4 (0.10 ml) + KOH (0.10 ml) → 175 °C, 48 hours.	monoclinic $P2_1/n$; a = 5.3999 b = 13.1644 c = 7.4117 β = 10.7.50; V = 502.48.	MnF_4O_2 octahedra in chains, and cross-linked by PO_3F tetrahedra into **2D** sheets separated by NH_4^+/K^+ ions.
$CsMnF_2(PO_3F)$ (JMN10)	MnF_3 (0.0842 g) + H_3PO_4 (0.10 mL) + CsOH (0.20 mL) → 175 °C, 48 h. Major crystalline phase ~70% remainder unidentified powder. Yield = 0.1160 g.	orthorhombic $C222_1$; a = 9.6876 b = 11.7081 c = 10.0105; V = 1135.42	MnO_3F_3 octahedra sharing vertices form helical chains cross-linked by PO_3F tetrahedra forming a **3D** framework with 2D orthogonal channels containing Cs^+ ions.
$Mn(II)_2PO_4F$ (JMN53)	MnF_3 (0.0842 g) + H_3PO_4 (0.10 mL) + ethylenediamine (0.08 mL) → 175 °C, 72 h. Minor crystalline phase ~40%. Yield = 0.0434 g.	monoclinic $C2/c$; a = 13.4233 b = 6.5079 c = 10.0939 β = 120.118; V = 762.73	Strongly distorted MnO_4F_2 octahedra sharing edges linked by PO_4 tetrahedra in a dense **3D** network.
$[H_2EDA]$ $FeF_3(PO_3F)$ EDA= ethylenediamine (JFE65)	FeF_3 (0.0960 g) + H_3PO_4 (0.10 mL) + ethylenediamine (0.08 mL) → 175 °C, 72 h. Crystalline phase ~80% remainder unidentified known powder. Yield = 0.1476 g.	orthorhombic $P2_12_12_1$; a = 6.4649 b = 9.5098 c = 12.9436; V = 795.77.	**1D** structure formed as a ladder along a of alternating FeO_3F_3 octahedra + PO_3F tetrahedra pairs separated by protonated template molecular ions.
(H-DET) $FeF(HPO_4)_2$DET = Diethylenetriamine (JFE126)	FeF_3 (0.0960 g) + H_3PO_4 (0.10 mL) + diethylenetriamine (0.12 mL) → 175 °C, 48 h. Crystalline phase ~80%, remainder unknown powder. Yield = 0.1276 g.	monoclinic $P2_1/n$; a = 7.3046 b = 20.4660 c = 8.6816 β = 92.307; V = 1296.81	FeO_4F_2 octahedra form infinite **1D** chains through shared trans F^- ions, pairs of cis oxygen atoms on adjacent FeO_4F_2 octahedra are bridged by 2 x HPO_4; protonated DET between chains.
$Ba_{1.5}FeF_2(PO_2(OH,F)_2 \cdot H_2O$ (JFE63)	FeF_3 (0.0960 g) + H_3PO_4 (0.20 mL) + $Ba(OH)_2 \cdot 8H_2O$ (0.3628 g) → 175 °C, 72 h. Single phase. Yield = 0.2063 g.	monoclinic $C2/c$; a = 13.1579 b = 4.7786 c = 29.2021 β = 93.793; V = 1832.10	FeF_2O_4 octahedra linked into **1D** chains by $PO_2(OH,F)_2$ groups separated by Ba^{2+} and water molecules.
$[H_2$-(PPA)$_3]$ $[(Fe_2F)Fe(PO_3F)_4(PO_2F_2)_2]$- PPA=Propylamine (JFE176)	FeF_3 (0.0960 g) + H_3PO_4 (0.10 mL) + PPA(d = 0.719; 0.09 mL) → 175 °C, 72 h. Single phase. Yield = 0.1152 g.	monoclinic $P2_1/n$; a = 9.4946 b = 23.0315c = 14.7646 β = 95.577; V = 3213.36	$(FeO_5)_2F$ dioctahedral dimers, bridged through F, and FeO_6 octahedra are linked through PO_3F and PO_2F_2 groups into **2D** sheets in the ac plane and separated by template molecules along b. Isostructural materials with different amines/ layer separations also obtained.
$[H$-DABCO$]FeF_2(PO_3F)$ (JFE82)	FeF_3 (0.0960 g) + HPF_6 (0.16 mL) + DABCO (0.1290 g) → 175 °C, 72 h. Single phase. Yield = 0.0096 g.	monoclinic $P2_1/n$; a = 13.2911 b = 6.3517 c = 17.3555 β = 111.769; V = 1360.7.	FeO_3F_3 octahedra edge linked into $Fe_2O_6F_4$ dimers and connected into **2D** sheets through PO_4 groups. Protonated DABCO between sheets.

Table 1. Continued

product, (code)	synthesis conditions and product yield/purity	crystallographic structure: lattice type, space group, lattice parameters (Å) and (deg) and cell volume (Å^3)	key structure features[a]
[H-piperazine]$_2$FeF$_2$(PO$_3$F) (JFE83)	FeF_3 (0.0960 g) + HPF_6 (0.16 mL) (0.10 mL) + piperazine (0.0991 g) → 175 °C, 72 h. Single phase. Yield = 0.0412 g. Yield = 0.0412 g.	triclinic a = 6.2825 b = 6.8653 c = 7.9998 α = 99.068 β = 97.979 γ = 111.323; V = 310.11	**2D** sheets of the same composition and connectivity as JFE82 − separated by protonated piperazine template molecular ions.
$Na_3Fe_2F_3(PO_4)_2$ (JFEJ11)	FeF_3 (0.0960 g) + H_3PO_4 (0.10 ml) + NaOH (0.06 ml) → 175 °C, 72 h. Single phase. Yield 0.1648 g.	Tetragonal $I4/mmm$; a = 6.3845 c = 10.6320; V = 433.38	**3D** framework isostructural with $Na_3V_2OF_2(PO_4)_2$[28]
$RbFeF_2(PO_3(OH,F))$ (JFE31)	FeF_3 (0.0960 g) + HPF_6 (0.16 mL) + RbOH (0.14 mL) → 175 °C, 48 h. Single phase. Yield = 0.0458 g.	orthorhombic $C222_1$; a = 9.7441 b = 11.7095 c = 9.8584; V = 1124.83	**3D** framework isostructural with JMN10 with Rb^+ replacing Cs^+.
$(CH_3NH_3)FeFPO_4$ (JFE123)	FeF_3 (0.0960 g) + H_3PO_4 (0.10 mL) + N-(3-aminopropyl)-1,3-propane diamine (0.16 mL) → 175 °C, 48 h. Crystalline phase ~80%, remainder unknown powder. Yield = 0.1043 g.	orthorhombic $Pnna$; a = 12.9530 b = 10.6466 c = 6.4469; V = 889.06	Infinite chains of cis and trans F-bridged FeO_4F_2 octahedra cross-linked by PO_4 tetrahedra forming a **3D** framework defining an intersecting 3D small pore system containing the $CH_3NH_3^+$ ions.
$(NH_4)_3Fe(III)_4F_9(PO_4)_2$ (JFE32)	FeF_3 (0.0960 g) + HPF_6 (0.16 mL) + NH_3 solution (0.03 mL) → 175 °C, 48 h. Single phase. Yield = 0.0304 g.	monoclinic $P2_1/m$; a = 7.1286 b = 14.4550 c = 7.5552 β = 106.74; V = 745.52	FeO_2F_4 octahedra linked through vertices into tetrahedral units further linked through bridging F and PO_4 units into a **3D** framework delineating 8-membered ring channels containing NH_4^+ ions.
Fe_2FPO_4 (JFE147)	FeF_3 (0.0960 g) + H_3PO_4 (0.10 mL) + 1,2 dianilinoethane →175 °C, 48 h. Single phase. Yield = 0.1106 g.	monoclinic $C2/c$; a = 13.0275 b = 6.4910 c = 9.8909 β = 118.696;V = 733.66	Known **dense 3D** structure, zweissite[27]
$Ba_2Cu_2(PO_3F)F_6$(ECU227)	CuF_2 (0.0584 g) + HPF_6 (0.16 mL) + BaF_2 (0.222 g) → 175 °C, 2 days. Single phase. Yield = 0.0724 g.	monoclinic $P2_1/c$; a = 12.190 b = 7.348 c = 9.627 β = 102.89; V = 840.52	**0D** structure with units of $[(CuF_3)_2PO_3F]^{4-}$ formed from PO_3F linked through O to $CuOF_3$ square planes with Ba^{2+} between units.
[H_2- piperazine]$Cu_2(PO_2F_2)_2(PO_4)F$ (ECU428)	CuF_2 (0.0584 g) + HPF_6 (0.32 mL) + piperazine (0.0948 g) → 125 °C, 18 days. Single phase. Yield = 0.0210 g.	triclinic P-1; a = 6.340 b = 10.101 c = 11.557 α = 71.82 β = 79.01 γ = 76.90; V = 679.22	**1D** chains of edge sharing octahedra alternating between CuO_4F_2 and CuO_2F_4 surrounded by PO_2F_2/PO_4 tetrahedra and CuO_3F_2 square planes. The chains are separated by $[piperazine\text{-}H_2]^{2+}$.
$M_2Cu_3(PO_3F)_4$(ECU31 [NH_4], ECU261 [Rb])	ECU31: CuF_2 (0.0584 g) + HPF_6 (0.16 mL) + NH_4F (0.047 g) → 175 °C, 2 days. Single phase. Yield = 0.0523 g. ECU261: CuF_2 CuF_2 (0.0584 g) + HPF_6 (0.16 mL) + RbF (0.132 g) → 175 °C, 2 days. Single phase. Yield = 0.0684 g.	monoclinic $P2_1/c$; M=[NH_4] a = 7.825 b = 9.494 c = 9.117 β = 94.87; V = 674.82, M = Rb a = 7.749 b = 9.434 c = 9.219 β = 95.19° V = 671.20	**2D** layer structure with 2 × CuO_5 square based pyramids lined via *trans*-CuO_4 square planes to form triplets. These triplets are linked via O by PO_3F tetrahedra to form corrugated F-lined layers with interlayer NH_4^+/Rb^+.
$K_2Cu_3(PO_3F)_4$ (ECU391)	CuF_2 (0.0584 g) + HPF_6 (0.16 mL) + KF (0.073 g) → 175 °C, 10 days 50% purity, unknown impurity. Yield = 0.067 g.	monoclinic $P2_1/n$; a = 11.283 b = 5.107 c = 11.109 β = 105.21; V = 634.49	**2D** sheets of the same composition and connectivity as ECU31 but different distribution of cations between layers.

Table 1. Continued

product, (code)	synthesis conditions and product yield/purity	crystallographic structure: lattice type, space group, lattice parameters (Å) and (deg) and cell volume (Å^3)	key structure features[a]
$Cs_2Cu_3(PO_3F)_4$ (SCU41)	CuF_2 (0.0584 g) + HPF_6 (0.16 mL) + CsF (0.167 g) → 220 °C, 2 days. Single phase. Yield = 0.0112 g.	triclinic *P*1; *a* = 5.4162, *b* = 7.9362, *c* = 9.3034, α = 84.198, *β* = 73.305, *γ* = 71.229; *V* = 362.70	**2D** structure related to ECU391 but with distorted copper square-based pyramids.
$Na_3Cu_3(PO_3(OH,F))_3PO_4$ (ECU74)	CuF_2 (0.0584 g) + H_3PO_3 (0.1 mL) + NaOH (0.06 mL) → 175 °C, 2 days Single phase. Yield = 0.0536 g.	monoclinic *Cc*; *a* = 17.689 *b* = 5.003 *c* = 16.103; *β* = 117.04° *V* = 1269.33	**2D** layered structure 2 × CuO_5 square based pyramids lined via *trans*-CuO_4 square planes to form triplets. PO_4, $PO_3(F,OH)$ tetrahedra link the copper triplets via O with interlayer Na^+ and OH/F orientated between layers.
$[H_3NCH_2(CH_2)_2CH_2NH_3]$-$Cu_3(PO_3F)_4$ (ECU283)	CuF_2 (0.0584 g) + HPF_6 (0.32 mL) + 1,4-diaminobutane (0.11 mL) → 175 °C, 2 days. Single phase. Yield = 0.0154 g.	triclinic *P*-1; *a* = 5.791 *b* = 9.609 *c* = 16.330 α = 90.43 *β* = 94.28 *γ* = 99.98; *V* = 892.28	Pairs of edge sharing CuO_5 square based pyramids linked through O by PO_3F with F orientated into interlayer space to form **2D** sheets in the *ac* plane with protonated [1,4-diaminobutane] aligned parallel to *c* between sheets.
$[H_3NC_6H_{10}NH_3]_{0.5}Cu(PO_3F)F$ (ECU284)	CuF_2 (0.0584 g) + HPF_6 (0.32 mL) + *trans*-1, 4-diaminocyclohexane (0.126 g) → 175 °C, 2 days Single phase. Yield = 0.0951 g.	monoclinic $P2_1/c$; *a* = 11.097 *b* = 10.969 *c* = 6.101 *β* = 102.11 *V* = 762.05	**2D** layer structure with infinite chains of μ^2-F vertex sharing CuO_4F square-based pyramids in the *c* direction bridged by PO_3F tetrahedra though O. Layers are separated by protonated *trans*-1,4-diaminocyclohexane aligned along *a*.
$Na_2Cu_2(P_2O_7)F$(SCU77)	CuF_2 (0.0584 g) + H_3PO_3 (0.1 mL) + NaOH (0.06 mL) → 225 °C, 2 days; 50% purity, unknown impurity. Yield = 0.1921 g.	monoclinic *C*2/*c*; *a* = 15.7149, *b* = 4.7342, *c* = 9.4993, *β* = 99.705; *V* = 696.61	**2D** layered structure with Na^+ between the layers. The layers consist of pairs of edge-sharing copper square-based pyramids [CuO_4F] connected by pyrophosphate groups [P_2O_7] with fluoride anions orientated into interlayer space.
$Cs_2Cu_2(PO_3F)_2F_{0.5}[P(O,OH,F)_4]_x$ (SCU45)	CuF_2 (0.0584 g) + H_3PO_3 (0.1 mL) + CsOH (0.2 mL) → 220 °C, 2 days; 50% purity, unknown impurity. Yield = 0.2751 g.	triclinic *P*-1; *a* = 4.9335, *b* = 9.8397, *c* = 13.4704, α = 106.578, *β* = 90.456, *γ* = 90.610; *V* = 626.65	**2D** layered structure with Cs^+ and disordered discrete [$P(O,OH,F)_4$] groups between layers. Layers formed of disordered infinite chains of μ^2-F vertex sharing CuO_4F_2 octahedra in the *a* direction, with chains bridged by CuO_4 square planes and PO_3F tetrahedra with F orientated into the interlayer space.
$Rb_2Cu_3(PO_2F_2)_2(PO_3F)$ (ECU30)	CuF_2 (0.1744 g) + HPF_6 (0.22 mL) + RbOH (0.2 mL) + H_2O (4 mL) → 175 °C, 4 days. Single phase. Yield = 0.2712 g.	monoclinic $P2_1/n$; *a* = 5.383 *b* = 14.191 *c* = 15.888 *β* = 91.83; *V* = 1213.13	**3D** framework with Rb^+ filled 1D-channels in the *a* direction. The framework consists of infinite chains of CuO_4F square based pyramids and CuO_5F octahedra running parallel to the channels, which are bridged by PO_3F tetrahedra.
$MCu_3(PO_2F_2)(PO_3F)_2F_2$ (ECU228 [K], ECU230 [Rb])	ECU228: CuF_2 (0.0584 g) + HPF_6 (0.05 mL) + KF (0.0222 g) → 175 °C, 2 days. Single phase. Yield = 0.0334 g. ECU230: CuF_2 (0.0584 g) + HPF_6 (0.05 mL) + RbF (0.0406 g) → 175 °C, 2 days. Single phase. Yield = 0.0414 g.	monoclinic *C*2/*c*; M = K *a* = 18.972 *b* = 7.497 *c* = 7.766 *β* = 103.63 *V* = 1073.56; M = Rb *a* = 19.090 *b* = 7.572 *c* = 7.819 *β* = 103.68 *V* = 1098.19	Triplets of face-sharing CuO_4F_2 octahedra with μ^3-F and connected by PO_3F tetrahedra to form 2D layers. These are bridged by PO_2F_2 tetrahedra to form a **3D** structure with 2D pores in the *bc* plane filled with M^+.

Table 1. Continued

product, (code)	synthesis conditions and product yield/purity	crystallographic structure: lattice type, space group, lattice parameters (Å) and (deg) and cell volume (Å^3)	key structure features[a]
$Cu_5(PO_3F)_2(PO_2F_2)_2F_4$ (ECU234)	CuF_2 (0.0584 g) + HPF_6 (0.16 mL) + KPF_6 (0.232 g) → 175 °C, 2 days. Single phase. Yield = 0.0024 g.	monoclinic $P2_1/n$; a = 7.446 b = 7.602 c = 12.934 β = 93.24; V = 730.89	**dense 3D** framework structure formed from CuO_2F_4/CuO_3F_3 octahedra and PO_3F/PO_2F_2 tetrahedra
$[Triethylamine]_xCu_3(PO_4)(PO_2F_2)_2$ (ECU435)	CuF_2 (0.0584 g) + HPF_6 (0.32 mL) + triethylamine (0.15 mL) → 125 °C, 18 days. Single phase. Yield = 0.0042 g.	triclinic P-1; a = 6.148 b = 9.251 c = 9.646 α = 64.02 β = 73.86 γ = 73.40 V = 465.08	**dense 3D** framework structure consisting of chains of distorted CuO_3F_2, CuO_4F and CuO_2F_3 square planes, linked by PO_4/PO_2F_2 tetrahedra.

[a] Dimensionality given in bold and compounds arranged in the order 1D → 2D → open 3D → dense 3D.

pyramids producing channels containing the protonated amine and, between the stacked $[Co(II)(PO_3F)]_4F$ cuboids, isolated H_2O molecules or F^- anions.

Metal Fluorophosphate 5; $(NH_4)(MnF_2PO_3F)$. (Table 1, compound JMN16). The structure of $[NH_4]^+[MnF_2PO_3F]^-$, Figure 3a, consists of layers of MnO_4F_2 octahedra linked into chains through fluoride and then into layers with the oxygen atoms of the PO_3F tetrahedra; the fluoride atoms of the PO_3F tetrahedra are directed into the interlayer region and form hydrogen bonds to the ammonium ions that separate the $[MnF_2PO_3F]^-$ layers.

Metal Fluorophosphate 6; $Na_4Mn_2F_6(P_2O_7)$. (Table 1, compound JMNJ15). The structure of $Na_4Mn_2F_6(P_2O_7)$, Figure 3b, consist of chains, along the (101) direction, formed from MnF_2O_4 octahedra linked through bridging P_2O_7 pyrophosphate anions on their *trans* edges. The two remaining oxygen atoms on the pyrophosphate groups link through the trans oxygen positions on MnO_2F_4 octahedra to form a 3D framework with channels along the three orthogonal directions and containing the sodium ions.

Metal Fluorophosphate 7; $MCu_3(PO_2F_2)(PO_3F)_2F_2$, M = K, Rb. (Table 1 compounds ECU 230 and ECU 228). The structure of $MCu_3(PO_2F_2)(PO_3F)_2F_2$, Figure 4a, comprises two types of copper-centered polyhedral units; one copper atom has a CuO_2F_2 or CuO_4F_2 local geometry with 2 short *trans* Cu−F (1.899 Å) and two short *trans* Cu−O (1.979 Å) distances plus two longer (2.37 Å) *trans*-Cu−O distances while the other has 5 + 1 × F coordination geometry with the main square-based pyramid consisting of a square-planar CuO_4 unit and apical fluoride. The $Cu(O,F)_n$ polyhedra link together through corners, edges, and faces with PO_3F tetrahedra to form layers which are then cross-linked by PO_2F_2 (possibly $PO_2(OH,F)_2$) tetrahedra to produce channels containing the potassium (rubidium) cations.

Metal Fluorophosphate 8. $M_2Cu_3(PO_3F)_4$ (Table 1 M = $[NH_4]$, ECU31; M = Rb ECU261). The structure of $M_2Cu_3(PO_3F)_4$ Figure 4b, consists of units of three linked copper centers, comprising a central CuO_4 square plane trans-linked through the oxygen to two CuO_5 square based pyramids, which are then cross-linked into slightly corrugated layers by PO_3F tetrahedra. The fluorine atom of the PO_3F tetrahedron is directed into the interlayer region and forms a hydrogen bond with the interlayer NH_4^+; $Rb_2Cu_3P_4O_{12}F_4$ is isostructural with a slightly smaller unit cell volume.

4. FURTHER CHEMISTRY—*CHIMIE DOUCE*

Potential applications of metal fluorophosphates include lithium insertion materials as positive electrode materials for Li-ion batteries and as nanoporous redox systems for catalysis. For lithium insertion hosts a channel or interlayer regions into which lithium can intercalate with concomitant reduction of a metal center in the framework/layer are the key features. Alternatively a lithium-containing derivative is needed for oxidative delithiation as a positive-electrode; this can be obtained through ion exchange of A^+ by Li^+ in a parent $A_a[[MO_nF_{6-n}]_x[PO_{4-m}F_m]_y$ phase. Ion exchange methods can replace larger (Na, K, Rb, Cs, and NH_4) or smaller (e.g., H^+ from PO_3OH or from alkylammonium ion thermal decomposition) with lithium. Reactions of this type have been used frequently for the production of positive-electrode materials; for example $LiMnO_2$[21,22] and Li_2FePO_4F[10] are obtained by ion exchange from sodium-containing parent materials and the insertion electrode material "Fe(III)PO_4" is formally derived from LiFe(II)PO_4 by oxidative lithium deinsertion. The generation of porous materials, of interest for catalysis as with zeolite chemistry, typically involves pyrolytic destruction of amine template molecular ions thus producing open framework or layer materials. To demonstrate the feasibility of such reactions with the new metal fluorophosphate materials the *chimie douce* of some compounds from Table 1 was investigated.

4.1. Removal of Extra-Framework Species. Materials having structures containing extra-framework species, such as ammonia or alkylammonium cations, were further investigated with respect to decomposition and removal of these species. Combined thermogravimetric and differential analysis in air showed that the ammonium or alkylammonium template is generally oxidized and lost from the structure at between 300 and 450 °C, (Caution: HF(g) may be generated) and the residual frameworks remained intact until typically 450 °C (PXD patterns collected from materials heated at 450 °C for 24 h show the same form as those of the parent material), see Supporting Information (S3). Further thermal decomposition occurs at higher temperatures (typically >600 °C) leading to the collapse of the porous/layered structure initially to amorphous intermediates which recrystallize to mixtures of metal phosphates and metal fluorides or new dense, complex metal fluoride phosphate phases; while not investigated further in this work these new condensed metal fluorophosphates could themselves be of interest as, for example,

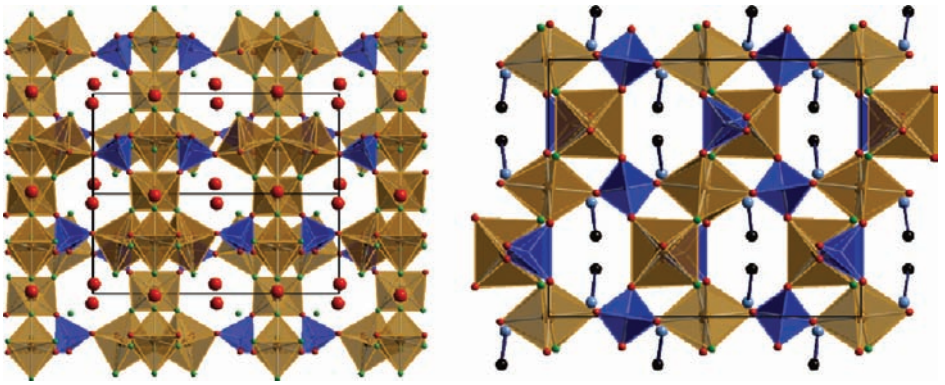

Figure 1. (a) Left. The structure of $(NH_4)_3Fe(III)_4F_9(PO_4)_2$ viewed between the *a* and *c* directions showing the channels containing the ammonium ions (nitrogen, large red spheres). Phosphate tetrahedra (blue) FeO_2F_4 octahedra (gold) (oxygen, small red spheres; fluorine, small green spheres). (b) Right. The structure of $(CH_3NH_3)FeFPO_4$ viewed down the *c* lattice direction showing the channels containing the methylammonium cations (no hydrogen shown, carbon, black; nitrogen, pale blue).

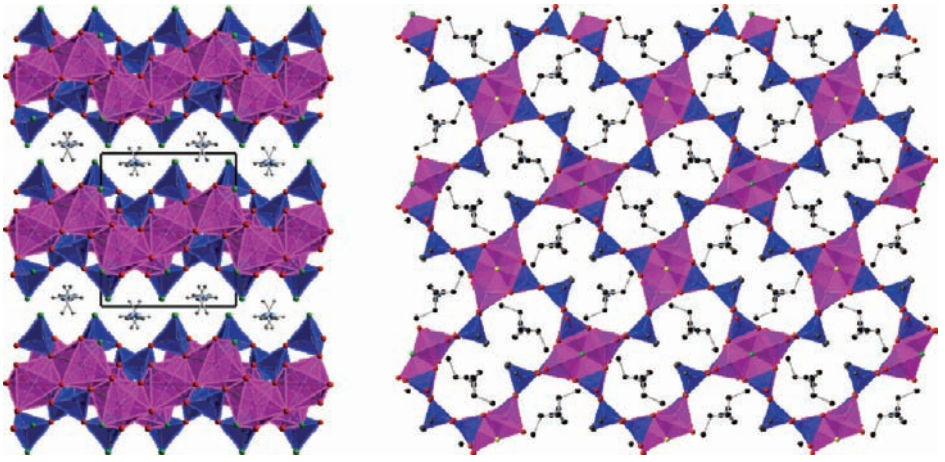

Figure 2. (a) Left. The structure of $NH_4Co(II)_3F_2(P_2O_6F)_2$ viewed down the *c* lattice direction showing the layers formed from P_2O_6F fluoropyrophosphate double tetrahedra (blue) and $Co(O,F)_6$ octahedra (magenta) (oxygen, small red spheres; fluorine, small green spheres) separated by ammonium cations (hydrogen, gray; nitrogen, pale blue). (b) Right. The structure of $[H_2{-}N\text{-}(2\text{-aminoethyl})\text{-}1,3\text{-propane-diamine}]_2^{3+}$ $[Co(II)(PO_3F)]_4F[PO_2F_2]_2.\{H_2O,F\}$ viewed down the *c* lattice direction: key as panel a with carbon shown as black spheres and water molecules/free fluoride as yellow spheres.

insertion hosts for positive electrode materials in Li-ion batteries. Thermogravimetric analysis in flowing nitrogen showed similar decomposition pathways for the materials studied in air, though residual carbon was often present in the products formed at 500 °C. For the cobalt(II) compounds, where no oxidation occurs in flowing nitrogen, small differences were found for equivalent samples heated in air but only above 470 °C where partial oxidation of cobalt(II) decomposition intermediates occurs.

4.2. Ion Exchange Reactions. Exchange of extra-framework cations was investigated via three routes: (i) stirring the metal fluorophosphate with a large molar excess of lithium as a $LiBF_4$ acetonitrile solution at 50 °C for 24 h, (ii) stirring with 2 M LiCl in water at 50 °C for 24 h and (iii) using a Li^+ ion flux of molten $LiBF_4$ at 300 °C under nitrogen. In a typical solution reaction 0.05 g of $CsMnF_2PO_3F$ (JMN10) was stirred with (a) 0.5 g of $LiBF_4$ dissolved in 5 mL of acetonitrile or (b) 2 M LiCl(aq). Products were analyzed by PXD and by SEM/EDAX, (see Supporting Information, S3 and S4). EDAX confirmed that cesium was removed in varying degrees from the metal fluorophosphate under all these conditions forming $[Cs]_{1-x}[Li(H_2O)_n]_xMnF_2PO_3F$ (n = 0 for nonaqueous systems). PXD data confirmed that the framework structure remained intact with only minor changes in lattice parameters but significant changes in peak intensities consistent with partial replacement of Cs^+ by Li^+ (see Supporting Information, S4). Similar lithium ion exchange reactions were successfully undertaken for many other materials described in Table 1 that have extra-framework cations.

4.3. Li Insertion—Reaction with LiI and Electrochemical Insertion. Reductive lithium insertion reactions were investigated using chemical and electrochemical methods. Various materials of the iron(III), manganese(III), and copper(II) fluorophosphates were stirred with LiI in dry acetonitrile at 50 °C. All Mn(III) fluorophosphates liberated iodine immediately (without decomposition) indicating rapid lithium insertion and reduction of the metal in the framework and concomitant oxidation of iodide to iodine. Most Fe(III) and Cu(II) fluorophosphates also

dx.doi.org/10.1021/ja201096b |*J. Am. Chem. Soc.* 2011, 133, 8252–8263

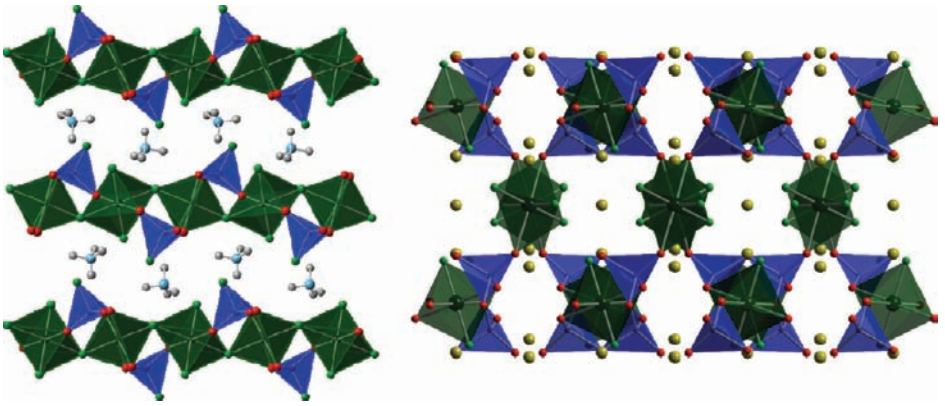

Figure 3. (a) Left. The structure of $[NH_4][MnF_2PO_3F]$ viewed down the *a* lattice direction showing PO_3F tetrahedra (blue) and MnO_4F_2 octahedra (dark green) (oxygen, small red spheres; fluorine, small green spheres); (b) Right. $Na_4Mn_2F_6(P_2O_7)$ viewed between the *a* and *c* axes showing MnF_4O_2 (center) and MnO_4F_2 octahedra and P_2O_7 ditetrahedral pyrophosphate anions; key as panel a with sodium as yellow spheres.

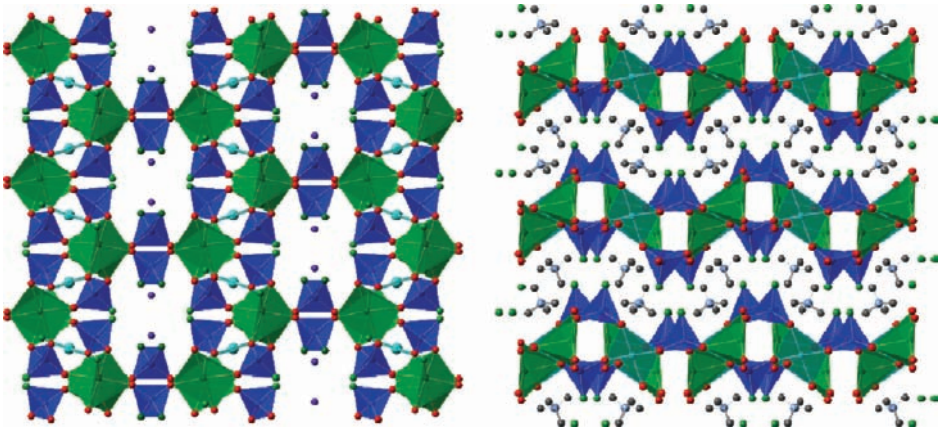

Figure 4. (a) Left. The structure of $MCu_3(PO_2F_2)(PO_3F)_2F_2$, M = K, Rb viewed down the *c* lattice direction showing PO_3F and PO_2F_2 tetrahedra (blue), CuO_4 square planes (cyan), and CuO_5 square-pyramids (green) (oxygen atoms, small red spheres; K/Rb, small purple spheres; fluorine, small green spheres). (b) Right. The structure of $M_2Cu_3(PO_3F)_4$ viewed down the *c* lattice direction showing PO_3F tetrahedra (blue), CuO_4 square planes (cyan), and CuO_5 square-pyramids (green) (oxygen, small red spheres; fluorine, small green spheres).

liberated iodine though less rapidly. The liberation of iodine consistent with oxidation at a potential of 2.8 V versus lithium metal; this supports the concept that these materials benefit from the electronegative and inductive effects of fluoride and phosphate, respectively, and would thus deliver useful cell voltages in a Li-ion cell. One material, JFE31 $CsFe(III)F_2(PO_3F)$, was selected for electrochemical testing and demonstrated a cell potential of ~3 V vs Li (see Supporting Information, S5), extensive further work is in progress to investigate the potential of these materials in the Li-ion batteries and will be reported in due course.

5. MAGNETIC SUSCEPTIBILITY

Three materials have been studied to date ECU31, ECU74, and JMN10; full details of the measurements are given in the Supporting Information (S6). ECU31 and ECU74 both contain triplets of copper centers formed from the polyhedral units $Cu(1)O_4-O-Cu(2)O_2-O-Cu(3)O_4$, that is, square pyramidal−square planar− square pyramidal. This type of triplet unit is reasonably well-known in molecular structures.[23] In ECU31 the unit is symmetric, that is Cu(1) is crystallographically equivalent to Cu(3), while in ECU74 their environments differ slightly. The arrangement of these triplets relative to each other is markedly different in the two materials and as a result the low temperature magnetic susceptibility data exhibit diverse characteristics. In both fluorophosphates the strongest antiferromagnetic interactions are within the triplet, and the Weiss constants derived for both materials (−54 K (ECU74) and −97 K (ECU31)) are indicative of this behavior. However, at the lowest temperatures the intertriplet interactions are weakly antiferromagnetic in ECU31, $T_N \approx 40$ K, while they are ferromagnetic in ECU74 ($T_C = 11.3$ K). This difference is likely to be associated with the much shorter intertriplet distances in ECU74 (two Cu−Cu intertriplet distances of 3.61−3.63 Å) compared with ECU31 (single shortest Cu−Cu intertriplet distance is 3.85 Å). Magnetic susceptibility data from JMN10 ($CsMn(III)F_2PO_3F$) show antiferromagnetic ordering at low temperature with $T_N = 13.9$ K. Differences in the field cooled and zero-field cooled data indicate some irreversibility in the system which may be associated with weaker magnetic interactions between the separate helical chains formed of linked $Mn(III)O_3F_3$ octahedra.

dx.doi.org/10.1021/ja201096b |*J. Am. Chem. Soc.* 2011, 133, 8252–8263

6. TRANSITION METAL FLUOROPHOSPHATES. OVERVIEW OF SYNTHESIS, COMPOSITION, STRUCTURE, AND CHARACTERISTICS

By increasing the fluoride content of reaction media involving first row transition metals, the fluoride ion can be readily incorporated into new materials formed from linked $M(O,F)_n$ and $P(O,F)_4$ polyhedra. The composition of these materials can be controlled to some extent through variation of the fluorine to oxygen ratio in the reaction medium, which is then reflected in that of the product; fluoride species used in this work included the metal fluoride, a counterion salt such as MF (M = Li−Cs, alkyl ammonium ion), HPF_6, or additional HF. High fluoride levels in the reaction media produced materials with more terminated polyhedra leading to lower dimensional structures with layers (2D), chains (1D), and discrete clusters (0D), Table 1; this behavior reflects that seen previously for the early transition metal fluorophosphates[16] and templated complex metal fluorides.[19] Two new features involving fluoride were found in this study, specifically: (i) the preference for fluoride to adopt bridging sites, frequently μ^2 but more rarely μ^3 and even μ^4 between metal ions (or, for μ^2, rarely between metal and phosphorus) and (ii) the formation of PO_3F and more rarely PO_2F_2 linking polyhedral units. The propensity for structures to contain bridging fluoride, a behavior not seen for the early transition metal compounds,[16] probably derives from the lower charge on the metal (3+ (Mn, Fe) and 2+ (Co and Cu) as opposed to 4+ and 5+ (Hf, Nb)) and the high positive charge that would otherwise derive on fully, or near-fully, connected 2-D or 3-D frameworks with M^{5+} in association with bridging monovalent anions rather than divalent ones. With di- and trivalent metals a framework with low overall negative charge can still result even with significant levels of bridging fluoride ions. In high fluoride concentration, reaction media products were often found to contain the fluorophosphate species PO_3F and PO_2F_2 (possibly also $PO_2(OH,F)_2$); the atom linking metal to phosphorus was normally oxygen though in a few cases M−F−P bridges were identified. The presence of PO_3F as a framework forming species is relatively unusual but was quite prevalent in the compounds isolated in this work; the three oxygen atoms most frequently formed part of the linked polyhedral structure with the fluoride ion terminal, and generally oriented toward a channel or interlayer region, *vide infra*.

Other features of the fluorophosphates produced in this work, and relevant to possible applications, such as positive-electrode materials, and interest in new magnetic materials, are worthy of discussion. With iron, manganese and copper the oxidation state of the starting material (+3 for Mn and Fe and +2 for Cu) was reflected in that of the products. In most cases in reactions with CoF_3 as a starting material reduction generally took place during the reaction, producing Co(II) fluorophosphates. This behavior with cobalt may be a consequence of a small level of water or an amine structure directing agent in the reaction mixture which readily reduces Co(III) to Co(II). The use of fluoride as a ligand should aid in the stabilization of high oxidation states, through its π and σ donor properties, and this would allow the targeting of even more highly oxidized metal centers in fluorophosphates in nonaqueous conditions; while not reported here V(IV) and V(V) fluorophosphates have been readily obtained using similar hydrofluorothermal methods.

Another feature of interest of the fluorophosphates is the frequent distribution of fluoride ions as terminal species on the metal polyhedral or fluorophosphate groups; this acts to "break-up" the structures with M−F or P−F oriented toward channels or interlayer regions, Table 1. Where charge balancing cations or alkylammonium cation templates are present in these regions ionic interactions or hydrogen bonds often exist between the group I/II metal or template cations and the terminal fluoride ion. Because of the lower charge on fluoride, compared with oxide in a framework formed solely from oxo-polyhedral species, these Coulombic interactions would be expected to be relatively weak, and so these fluoride lined channels or interlayer regions may provide facile pathways for small ion (e.g., Li^+ or Na^+) mobility.

While electron conduction in structures formed from transition metal and fluoride ions is generally lower than in metal oxide systems, due to the more electronegative fluoride ion producing a larger band gap, one feature of the fluorophosphates discovered in this study is the propensity for structures containing metal-centered, edge-sharing polyhedra. This structural feature, which is also present in $LiFePO_4$, may provide a route to improved electrical conductivity.[24] The incorporation of alkylammonium template ions into the channels and interlayer regions of many of the structures provides an alternative mechanism by which electron transfer in these materials could be enhanced; pyrolysis of the materials in anaerobic conditions leads to decomposition of the organic template leaving residual carbon in the channels and interlayer regions, as found for materials for which TGA data were collected under flowing nitrogen.

Initial magnetic susceptibility measurements on some of the compounds described in Table 1 show some intriguing behaviors. So while ECU31 and ECU74 have a similar structure feature containing copper, differences in the distribution of the triplets of CuO_n polyhedra lead to ferromagnetic interaction only in ECU74. Many of the other copper(II) fluorophosphates, for example compound ECU428, contain clusters and chains of edge-sharing metal polyhedra equivalent to 1-D Heisenberg chains. Other materials show structural features typical of frustrated systems; for example JFE32 (which we have as yet been unable to obtain as a fully pure phase needed for magnetic susceptibility studies) contains four iron centers forming a tetrahedral cluster that are then linked by two corners of the supertetrahedron into an infinite chain. Some of the materials crystallize in polar or chiral space groups and contain highly polarizable cations (e.g., Cs^+) and asymmetric metals centers (an additional feature of $M(O,F)_n$ polyhedra). Further investigations of the magnetic and nonlinear optical properties of these new metal fluorophosphates are also in progress.

7. DISCUSSION

Synthesis in hydrothermal conditions in the presence of high levels of fluoride leads to the formation of a very large new class of mid- to late-first row transition metal fluorophosphates. The additional composition flexibility granted by combining and linking different transition metal centered $M(O,F)_n$ and $P(O,F)_n$ polyhedra in the presence of templating or framework charge balancing cations leads to great structural variation in the materials formed. Further variation in the nature of the template, reaction temperature, solvent, reactant concentrations, and other reaction parameters is possible, and such work is likely to significantly enlarge this family of materials still further. It would also be possible to target other transition metals (e.g., Ni) and oxidation states (e.g., Co(III)) in further synthesis work, particularly by extension to more oxidizing solvothermal

conditions. Structures containing $As(O,F)_4$ tetrahedra linked with $M(O,F)_n$ polyhedra can also be produced either as new topologies or as analogues of many of the compounds presented in Table 1.

Advantages of fluoride-rich hydrofluorothermal synthesis include the ability to stabilize more unusual oxidation states in the products, for example Mn(III) from the commercially available MnF_3, though perhaps more important is that the route allows facile and relatively safe (compared with the use of high concentrations of HF) incorporation of high levels of fluoride into the products, which as a result then contain species such as $[MO_3F_3]$ and $[PO_2F_2]$. The linking of these fluoride-rich polyhedra is markedly different from pure oxo-polyhedra leading to new structural motifs such as channels and interlayer regions lined with fluoride ions, low-dimensional metal centered chains, and bridging fluoride between metal centers. Using the hydrofluorothermal methodology described herein, additional structural and compositional flexibility now exists for key transitional metals such as Mn(III), Fe(III), Co(II), and Cu(II) whose compounds have widespread applications in energy storage devices, magnetic materials, and in catalysis.

■ ASSOCIATED CONTENT

Supporting Information. (1) Synthesis conditions and experimental methods: (a) generic synthesis methods for transition metal fluorophosphates; (b) detailed synthesis parameters for JMN10, $CsMnF_2PO_3F$; (c) detailed synthesis parameters for JCO140, $[H_2{-}N$-(2-aminoethyl)-1,3-propane-diamine$]_2$ $[Co(II)(PO_3F)]_4F[PO_2F_2]_2.(H_2O,F)$; (d) experimental methods and instrumentation. (2) Thermogravimetric/differential thermal analysis data for representative compounds. (3) SEM images and EDAX data for representative compounds. (4) Li-ion exchange of $CsMnF_2PO_3F$ (JMN10), powder X-ray diffraction patterns before and after exchange, SEM images/EDAX data before and after exchange. (5) Cyclic voltammogram for discharge of Li into JFE31 $CsFe(III)F_2(PO_3F)$/carbon black. (6) CIFs for metal fluorophosphates 1−8. (1) $(NH_4)_3Fe(III)_4F_9(PO_4)_2$ (Table 1, compound JFE32). (2) $(CH_3NH_3)FeFPO_4$ (Table 1, compound JFE123). (3) $(NH_4)(Co(II)_3F_2(P_2O_6F)_2)$ (Table 1, compound JCO152). (4) $[H_2{-}N$-(2-aminoethyl)-1,3-propane-diamine$]_2$ $\{[Co(II)(PO_3F)]_4F[PO_2F_2]_2.(H_2O,F)\}$ (Table 1, JCO140). (5) $(NH_4)(MnF_2PO_3F)$ (Table 1, compound JMN16). (6) $Na_4Mn_2F_6(P_2O_7)$ (Table 1, compound JMNJ15). (7) $MCu_3(PO_2F_2)(PO_3F)_2F_2$, M = K, Rb (Table 1 compounds ECU 230 and ECU 228). (8) $M_2Cu_3P_4O_{12}F_4$ (Table 1 M = $[NH_4]$, ECU31; M = Rb ECU261. This material is available free of charge via the Internet at http://pubs.acs.org.

■ AUTHOR INFORMATION

Corresponding Author
mtw@soton.ac.uk

■ ACKNOWLEDGMENT

We thank EPSRC for allied funding under EP/F013752/1, John Owen and Matthew Roberts for the preliminary electrochemical measurements, Edward Young for the collection of the magnetic susceptibility data, and Mark Light for assistance with some aspects of the structure solution from single crystal data.

■ REFERENCES

(1) Natarajan, S.; Mandak, S. *Angew. Chem., Int. Ed.* **2008**, *47*, 4798.
(2) Barrer, R. M. *Hydrothermal Chemistry of Zeolites*; Academic Press: London, 1982.
(3) Wilson, S. T.; Lok, B. M.; Mesina, C. A.; Cannan, T. R.; Flanigen, E. D. *J. Am. Chem. Soc.* **1982**, *104*, 1146.
(4) Clearfield, A. *Curr. Opin. Solid State Mater. Sci.* **1996**, *1*, 268 and references therein.
(5) Cheetham, A. K.; Férey, G.; Loiseau, T. *Angew. Chem., Int. Ed.* **1999**, *38*, 3268.
(6) Padhi, A. K.; Nanjundaswamy, K. S.; Goodenough, J. B. *Electrochem. Soc. Meet. Abstr.* **1996**, *96−1*, 73.
(7) Hagman, L. O.; Kierkegaard, P. *Acta Chem. Scand.* **1968**, *2*, 1822.Boilot, J. P., Collin, G.; Colomban, P. *Energy, Mines and Resources*; Natural Resources Canada: Ontario, Canada, CANMET ERP/MSL 83-94(TR), 1983, 91.
(8) Rocha, J.; Lin, Z. *Rev. Miner. Geochem.* **2005**, *57*, 173. Nyman, M.; Gu, B. X.; Wang, L. M.; Ewing, R. C.; Nenoff, T. M. *Microporous Mesoporous Mater.* **2000**, *40*, 115.
(9) Clearfield, A.; Thakur, D. S. *Appl. Catal.* **1986**, *26*, 1.
(10) Ellis, B. L.; Lee., K. T.; Nazar, L. F. *Chem. Mater.* **2010**, *22*, 691.
(11) Barker, J.; Saidi, M. Y.; Swoyer, J. L. *Electrochem. Solid-State Lett.* **2003**, *6*, A1.
(12) Ellis, B. L.; Makahnouk, W. R. M.; Makimura, Y.; Toghill, K.; Nazar, L. F. *Nat. Mater.* **2007**, *6*, 749.
(13) Barker, J.; Gover, R. K. B.; Burns, P.; Bryan, A. J. *Electrochem. Solid-State Lett.* **2006**, *9*, A190. Kirsch, J. E.; Izumi, H. K.; Stern, C. L.; Poeppelmeier, K. R. *Inorg. Chem.* **2005**, *44*, 4586.
(14) Dance, J.-M. Tressaud, A. *Inorganic Solid Fluorides: Chemistry and Physics*; Hagenmuller, P. Ed.; Academic Press: Orlando, FL, 1985; Chapter 9.
(15) Murthy, J. K.; Gross, U.; Rüdiger, S.; Ünveren, E.; Kemnitz, E. *J. Fluorine Chem.* **2004**, *125*, 937.
(16) Rouse, J.; Redrup, K. V.; Kotsapa, E.; Weller, M. T. *Chem. Commun.* **2009**, *46*, 7209.
(17) Bonhomme, F.; Thoma, S. G.; Rodriguez, M. A.; Nenoff, T. M. *Chem. Mater.* **2001**, *13* (6), 2112–2117. Lakiss, L.; Simon-Masseron, A.; Porcher, F.; Patarin, J. *Eur. J. Inorg. Chem.* **2006**, 237–243. Estermann, M.; McCusker, L. B.; Baerlocher, Ch.; Merrouche, A.; Kessler, H. *Nature* **1991**, *352*, 320. Férey, G. *J. Fluorine Chem.* **1995**, *72*, 187.
(18) Riou-Cavellec, M.; Riou, D.; Férey, G. *Inorg. Chem. Acta* **1999**, *291*, 317. Riou-Cavellec, M.; Grenèche, J.-M.; Férey, G. *J. Solid State Chem.* **1999**, *148*, 150.
(19) Adil, K.; Leblanc, M.; Maisonneuve, V.; Lightfoot, P. *Dalton Trans.* **2010**, *39*, 5983.
(20) Sauvage, F.; Bodenez, V.; Vezin, H.; Albrecht, T. A.; Tarascon, J.-M.; Poeppelmeier., K. R. *Inorg. Chem.* **2008**, *47* (19), 8464.
(21) Tajimi, S.; Ikeda, Y.; Uematsu, K.; Toda, K.; Sato, M. *Solid State Ionics* **2004**, *175*, 287.
(22) Armstrong, A. R.; Bruce, P. G. *Nature* **1996**, *381*, 499.
(23) Removic-Langer, K.; Haussuhl, E.; Wichl, L.; Wolf, B.; Sauli, F.; Hasselmann, N.; Kopietz, P.; Lang, M. *J. Phys. Condens. Mater.* **2009**, *21*, 185013.
(24) Chung, S.-Y.; Bloking, J. T.; Chiang, Y. M. *Nat. Mater.* **2002**, *1*, 123.
(25) Feng, P.; Bu, X.; Tolbert, S. H.; Stucky, G. D. *J. Am. Chem. Soc.* **1997**, *119*, 2497.
(26) El Khayati, N.; Cherkaoui El Moursli, R.; Rodriguez-Carvajal, J.; Andre, G.; Blanchard, N.; Bouree, F.; Collin, G.; Roisnel, T. *Euro. Phys. J. B.* **2001**, *22*, 429.
(27) Yakubovich, O. V.; Simonov, M. A.; Matvienko, E. N.; Belov, N. V. *Doklady Akademii Nauk SSSR.* **1978**, *238*, 576.
(28) Sauvage, F.; Quarez, E.; Tarascon, J. M.; Baudrin, E. *Solid State Sci.* **2006**, *8*, 1215.